PAPER

Visible light photocatalysts—N-doped TiO$_2$ by sol–gel, enhanced with surface bound silver nanoparticle islands

Charles W. Dunnill,[a] Zarrin Ansari,[a] Andreas Kafizas,[a] Stefano Perni,[ab] David. J. Morgan,[c] Mike Wilson[b] and Ivan P. Parkin[*a]

Antimicrobial thin film photocatalysts consisting of N-doped titania have been prepared by sol–gel methods and further enhanced using silver nanoparticles formed *in situ* on the surface of the films. The films have been characterised using XRD, SEM, XPS, UV-Visible spectroscopy and functionally tested using measurements for the photoinduced superhydrophilicity, stearic acid destruction and anti-microbial measurements using both *E. coli* and an epidemic strain of MRSA, EMRSA-16. The N-doped TiO$_2$ films were seen to have interstitially doped nitrogen with the N 1s peak appearing at 400.0 eV in the XPS and as such showed good photocatalytic activity under white light. The photoactivity was then further enhanced by silver nanoparticle formations on the surface. The highly active photocatalytic films were seen to be effective agents against both bacteria and stearic acid using a white light source that is commonly found in UK hospitals.

1. Introduction

Visible light photocatalysts have varied applications with potential to provide solutions to some of the most poignant issues of the 21st century, such as the provision of safe clean drinking water[1,2] through photo-disinfection and the production of a renewable and carbon neutral energy source through the photo-splitting of water.[3] Another application is the prevention of hospital acquired infections where visible light photocatalysts could be used as anti-microbial and self-cleaning coatings under indoor lighting conditions as a preventative measure for hospital acquired infections. The Centre for Disease Control in the US (CDC) have reported that healthcare-associated infections are in the top ten leading causes of death in the United States,[4] with an estimated 1.7 million infections acquired annually, resulting in ∼99 000 deaths.[5] Figures for the UK show bacteria associated with healthcare-associated infections are recorded as a "signifi-cant factor" on over 7500 UK death certificates in 2008,[6] with an estimated cost the UK tax payer ∼£1 bn pa.[7] The contamination of frequently handled surfaces augments bacterial transfer and infection rates. These surfaces could be coated with an anti-microbial coating and help to reduce the spread of infection.

There is also much interest in photocatalyst applications for self-cleaning windows.[8,9] These windows traditionally work by the application of a thin film of TiO$_2$ which is functionalised by incident UV light (λ < 385 nm) and is responsible for the destruction of organic material through the generation of an electron–hole pair that, when reaching the surface, decomposes the organic substance into carbon dioxide water and mineral acids. The photo-induced formation of a superhydrophilic surface also plays an important part by allowing resulting matter and dirt to be uniformly washed off reducing the sheer amount of photo-destruction of organic matter that is necessary to achieve a clean sterile surface.

The functional properties of TiO$_2$ can be changed by tuning the band onset towards the visible region of the spectrum through doping, thus allowing for a photocatalyst that operates under indoor lighting conditions. A relatively small shift in the band onset would, therefore, have a significant improvement on the photocatalytic properties under white light conditions such as those commonly found in hospitals. The band onset shift can occur through many routes including the doping of inorganic elements into the lattice.

Elements such as nitrogen, sulfur, carbon and silver have been successfully incorporated into the TiO$_2$ structure by sputtering,[10] pulsed laser deposition,[11] CVD[12–16] and sol–gel synthesis.[17–22] Metals such as silver and gold have also been observed to enhance the photocatalytic and antimicrobial effect.[1,2,17,19,23–29] N-doped titania prepared by sol–gel produces effective visible light photocatalyst particles with properties that can be varied by altering the N : Ti : O ratio and the calcination tempera-ture.[18,21,22] This has been computationally calculated[10] and

[a] Centre for Materials Research, Department of Chemistry, University College London, 20 Gordon Street, London, UK WC1H 0AJ. E-mail: I.P.Parkin@ucl.ac.uk
[b] Division of Microbial Diseases, Eastman Dental Institute—University College London, 256 Gray's Inn Road, London, UK WC1X 8LD
[c] Cardiff Catalysis Institute—Cardiff University, Main building, Park Place, Cardiff, UK CF10 3AT

11854 | *J. Mater. Chem.*, 2011, **21**, 11854–11861

This journal is © The Royal Society of Chemistry 2011

experimentally shown to alter the band gap,[12,21,22,30] the crystal size and the functional properties. It is, however, as yet undecided which dopants form the most effective visible light photocatalyst, or the optimum concentration.

The bactericidal properties of silver ions have been investigated, and found to be effective against both Gram-negative and Gram-positive bacteria.[31] Gram-positive bacteria tend to be more susceptible to light activated agents but less susceptible to silver induced toxicity while the opposite is true for Gram-negative bacteria.[32–37] Silver ions can be absorbed by microbes from the material surface with a high degree of toxicity, thereby operating as a potent antimicrobial agent. The silver metal when in contact with bodily fluids can form Ag^+ which passes through bacterial cell walls and binds to some bacterial proteins, creating modifications of the cell wall membrane with fatal consequences to the bacteria.[38] This concept has been implemented on a range of commercial products including both open and enclosed surfaces such as catheter and ventilator tubing.[39] In addition to this a synergistic effect has been observed between TiO_2 and silver whereby the silver and the TiO_2 co-promote the antimicrobial effects of each other, producing a more potent antimicrobial surface that has potential to kill bacteria through a number of different pathways, reducing bactericidal resistance.[19] It has been shown that silver can promote the photoactivity of TiO_2 shifting the activity into the visible region.[19,23–25]

Here we prepare new interstitially N-doped TiO_2 films by sol–gel and incorporate silver nanoparticles onto the surface to produce enhanced visible light photocatalysts. The samples of N-doped TiO_2 were prepared with different sintering temperatures and dopant concentrations. These visible light photocatalysts have then been further enhanced using silver nanoparticles that were deposited on the surface *via* UV photo-assisted reduction of silver nitrate solution. The films provide strong evidence for visible light activated photoinduced superhydrophilicity. The antibacterial properties were assessed using EMRSA-16 as a representative Gram-positive organism and *E. coli* as a representative Gram-negative organism. EMRSA-16 is the most light tolerant of the two epidemic strains of MRSA currently affecting UK hospitals. We show that the primary kill mechanism for Ag–TiO_2 films is through the silver release however this process is significantly enhanced by the action of visible light from N–TiO_2.

2. Experimental methods

2.1 Thin film deposition

Samples were prepared using a sol–gel preparation consisting of acetylacetone, butan-1-ol, titanium *n*-butoxide and methyl ammonium chloride as a nitrogen source. The preparation was as used for pure TiO_2 but with the presence of the methyl ammonium chloride as a nitrogen source. Samples N1-400 and N1-500 were prepared as follows:

Acetylacetone (2.5136 g, 0.02514 mol) was dissolved in butan-1-ol (32 cm³, 0.035 mol) forming a clear colourless solution, to which titanium *n*-butoxide (14.22 g, 0.04 mol) was added. The solution was stirred for 1 hour, forming a clear pale yellow solution. Methyl ammonium chloride (1.00 g, 0.015 mol) dissolved in water (4.00 ml, 0.22 mol) was in turn dissolved in

isopropanol (9.07 g, 0.16 mol). This was added drop wise to the solution over a period of 5 minutes, with constant stirring. The sol remained clear but the colour became more intense. After stirring for one hour acetonitrile (1.67 g, 0.04 mol) was added drop wise with constant stirring. The solution was stirred for a final hour and allowed to age overnight before being used for dip-coating. The films were prepared on glass microscope slide substrates with two dips in the sol retracting at a rate of 120 cm min⁻¹, with the gel allowed to dry between each dip. The slides were heated (10 °C min⁻¹) in a muffle furnace to either 400 °C N1-400 or 500 °C N1-500 for 5 hours and allowed to cool to room temperature.

Samples N2-400 and N2-500 were prepared as in the case of N1 samples but with 2 g of methyl ammonium chloride used in the sol rather than 1 g. These had an initial molar ratio of Ti : N 1.4 : 1. Samples N2 therefore had twice the nitrogen content in the sol–gel deposition.

Slides from each sample were dipped in silver nitrate solution in methanol (5×10^{-3} M AgNO₃, Fisher Scientific) for 30 s withdrawn, left to air dry for 2 hours and then exposed to UV radiation (254 nm) for one hour in a light box. The resulting samples are labelled with the prefix Ag.

2.2 Characterisation techniques

X-Ray diffraction was achieved using a Bruker-Axs D8 (GADDS) diffractometer, utilising a large 2D area detector and a Cu X-ray source, monochromated (Kα1 and Kα2) fitted with a Gobble mirror. The instrumental setup allowed 34° in both θ and ω with a 0.01° resolution and 3–4 mm² of sample surface illuminated at any one time. Multiple Debye–Scherrer cones were recorded simultaneously by the area detector with two sections covering the 65° 2θ range. The Debye–Scherrer cones were integrated along ω to produce standard 1D diffraction patterns of 2θ against intensity. Scan data were collected for 800 s to give sufficiently resolved peaks for indexing. Scanning electron microscopy was performed using secondary electron imaging and back scattered imaging on a Hitachi S3400N instrument with an Oxford instruments EDX spectrometer attached. Samples were gold coated prior to imaging to reduce charging effects. A Perkin Elmer Lambda 25 UV-Visible Spectrometer was used to measure UV-Visible absorption and transmission spectra within the range of 1000–200 nm, yielding information on the band onset, the colour and the thickness of the films. Raman was achieved using a Renishaw inVia Raman microscope, and UV-Visible; transmission and reflectance measurements were achieved using a Perkin Elmer λ950. High resolution X-ray photoelectron spectroscopy (XPS) was performed on a Kratos Axis Ultra-DLD photoelectron spectrometer using monochromatic Al-K$_{\alpha}$ radiation at Cardiff University (EPSRC grant # EP/F019823/1). Survey spectra were collected at a pass energy of 160 eV, while narrow scans acquired at a pass energy of both 40 eV and 10 eV, the Kratos immersion lens neutralization system was used for charge neutralization of the samples. The data were analysed using CasaXPS™ software and calibrated to the C (1s) signal at 284.7 eV, attributed to adventitious carbon.

Water contact angle measurements were determined on a FTA 1000 contact angle measurement system. Samples were measured both prior to and post-irradiation by white light and UV light

with a drop of deionised water ~6.5 µl discharged from a Gauge 30 needle and photographed side on. Measurements were taken as an average of three readings.

The destruction of stearic acid was used to assess the photo-catalytic properties. A drop of stearic acid in methanol was applied to the surface of the films and allowed to dry into a greasy residue. The residues were monitored over time using IR spectroscopy under different lighting conditions using a PerkinElmer FT-IR Spectrum RX I Spectrometer 3000–2800 cm^{-1}. The lighting sources used for the photo-degradation studies were a UV light source and a white light source. This white light source is commonly found in UK hospital environments and has an intensity of 6000 lux at a distance of 20 cm from the samples as arranged in the light box. Details of the white light source, along with the spectral output, have previously been shown.[13] The stearic acid concentration was measured at 24 hour intervals and depicted by IR spectra.

2.3 Antibacterial assay

The organisms used were: methicillin-resistant *Staphylococcus aureus* EMRSA-16 and *Escherichia coli* ATCC 25922. These organisms were maintained by weekly subculture on Brain Heart Infusion (BHI) agar (Oxoid, Basingstoke, UK). For experimental purposes, the bacteria were grown aerobically in BHI broth (Oxoid) statically at 37 °C for 24 hours.

These cultures were centrifuged for 10 min at 2400g, the liquid was aseptically removed and the microbial cells resuspended in sterile phosphate buffer solution (PBS); this was repeated twice. Finally the cells were diluted 1 in 100 in PBS; the resulting bacterial suspensions contained approximately 10^7 CFU ml^{-1}.

The antimicrobial activity of the coated glass samples was then assessed using the following assay. Samples were placed into a plastic sterile BioAssay dish (Nalge Nunc Int. Corp., NJ, USA), a sheet of wet paper was added inside the box, without touching the samples, to prevent drying. An aliquot (50 µl) of the microbial suspension was carefully placed on the surface of the sample and a glass cover slip placed on top, experiments were performed on three independent cell cultures. The samples were incubated at 20 °C and either irradiated under white light (28 W, Biax 2D, General Electric) for 5 hours, or incubation for the same length of time in the dark in the case of controls. The irradiation had a light intensity of 1000 lux measured with Lutron Lx101 lux meter.

The glass was then placed in a 50 ml tube (Sarstedt) containing 450 µl of sterile PBS and vortexed for 1 minute; further serial dilutions were prepared in sterile PBS. Duplicate 25 µl aliquots of each dilution were then plated out onto either Mannitol Salt agar in the case of MRSA or MacConkey agar in the case of *E. coli*. All plates were incubated aerobically at 37 °C for 48 hours; survivors were then enumerated by viable counting.

3. Results and discussion

A number of N-doped TiO$_2$ thin films were prepared using sol–gel methods with varying nitrogen concentrations in the sol and varying sintering temperatures. The films were characterised with the two best performing photocatalysts further enhanced with
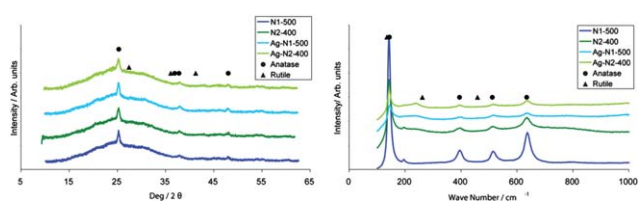

Fig. 1 XRD and Raman patterns for the films under investigation. Films were prepared by sol–gel synthesis, fired at 400 or 500 °C (**N1-500**, **N2-400**) and then further enhanced using silver nanoparticles (**Ag–N1-500**, **Ag–N2-400**).

silver nanoparticles. Similar crystallinity was observed between the samples.

3.1 Structural characterisation

X-Ray diffraction and Raman show that the films were predominantly anatase form of TiO$_2$ with no rutile signals (Fig. 1). XRD patterns were indexed to the tetragonal unit cell with cell constants: $a = 3.79(7)$ and $c = 9.50(8)$ Å.

Scanning electron microscopy (SEM) images of the films (Fig. 2) show a smooth surface with nanoparticulate islands in the case of silver. There was no discernible difference between the morphologies in **N1-500** and **N2-400** films or **Ag–N1-500** and **Ag–N2-400**. Samples sintered at 400 °C or 500 °C appear to have a similar appearance, indicating that heating at similar yet variant temperatures does not have a cosmetic effect upon the resulting films. The cracks are due to stress during the heating and cooling cycle of the sintering process due to thermal expansion differences between the film and the substrate.[19] The particles on the surface of **Ag–N2-400** were seen to be of higher density using the back scattered detector and EDX showed them to have a high silver content. The particles in Fig. 2 are observed to be about the same size as the particles observed in the AFM (Fig. 5).

UV-Visible-IR spectroscopy was carried out on all six samples (**N1-400**, **N2-400**, **N1-500**, **N2-500**, **Ag–N1-400**, **Ag–N2-500**) in both reflectance and transmission mode. The data were used to assess the thickness of the thin films, the colour and the band onset for the semiconductor material on the surface. The film thickness for each sample was found to be in the range 140–170 nm, calculated using the Swanepoel method from the reflectance data.[40] The Swanepoel method involves the analysis of the reflection data such that the interference pattern due to thickness can be related to the refractive index of the material.
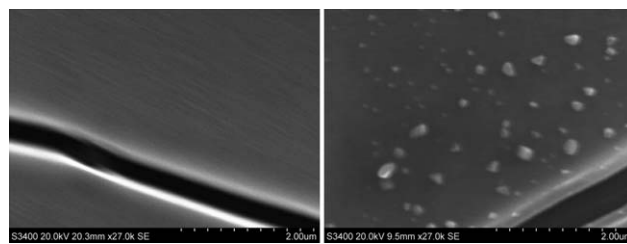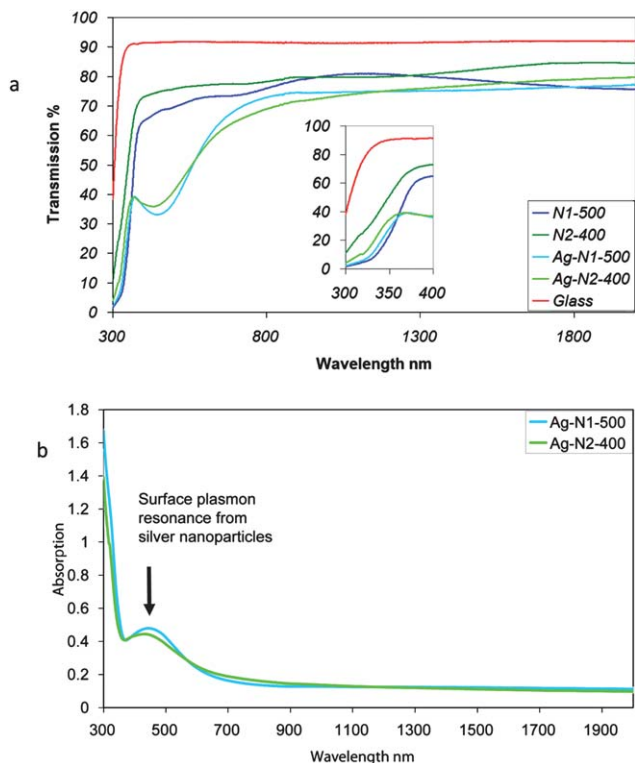

Fig. 2 SEM micrograph showing the surface of the the (a) **N1-500** film and (b) **Ag–N2-400** film. Both samples were exemplary of the silver and non-silver loaded samples.
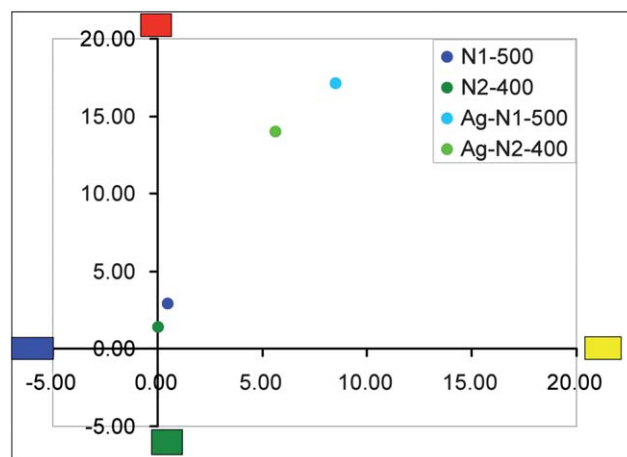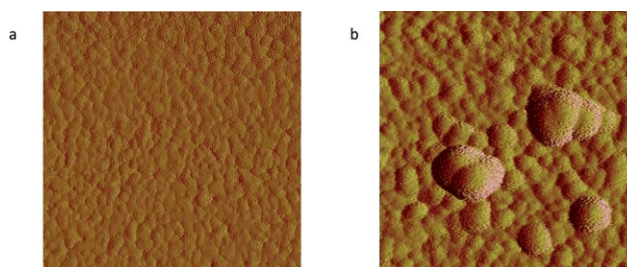
Table 1 The estimated band onset for the different films and the Lab* coordinates for their corresponding colours

Sample	Band onset energy/eV	L*	A*	B*	Dominant wavelength
N1-500	3.05	90.8	2.3	3.1	574
N2-400	3.05	93.5	0.3	1.3	571
Ag–N1-500	3.0	74.87	8.53	17.11	580
Ag–N2-400	3.0	75.47	5.66	14.01	578

Fig. 3 (a) UV-Visible-NIR transmission spectra for the different samples prepared by sol–gel methods. (b) Absorption spectra showing the surface plasmon resonance of the nanoparticles of silver on the surface of the films.

Fig. 4 Schematic of the LAB* coordinates for the different films showing the variation in colour. Lab* co-ordinates are a standard method of describing colour and consist of a luminosity value 0–100, followed by a scale factor for the red/green and blue/yellow.

Fig. 5 AFM area mapping of the (a) N–TiO$_2$ surface and (b) silver enhanced N–TiO$_2$ surface. Image width is 1 μm and $\frac{1}{2}$ μm length scales for the images respectively.

The thickness can therefore be estimated if the refractive index is known. Tauc plots[41,42] were used to estimate the band onset and consist of a plot of $(A*hv)^{0.5}$ against energy where A represents the absorbance of the material when the glass substrate is accounted for. The values for these are given in Table 1. All of the photocatalysts had a band onset around 3.0 eV. This indicates that the TiO$_2$ has been doped by the nitrogen resulting in a shift in the band onset from 3.2 eV. Similar syntheses at a lower sintering temperature of 250 °C showed a band onset of 3.2 eV as would be expected for TiO$_2$ in its pure anatase form. These films were not good photocatalysts under visible light conditions.

The colour variation in the films is negligible with Lab* co-ordinated as shown in Table 1 and in Fig. 4. The slight shifting to the yellow axis indicated the presence of minimal nitrogen doping,[12,14,15] and the shift to the red indicates the presence of the silver nanoparticles on the surface. Absorption spectra, Fig. 3(b), calculated from the transmission data show the surface plasmon resonance effects of the silver nanoparticles on the surface of the films indicating the presence of the silver. The SPR is red shifted

with respect to the 400 nm position that is often observed with silver nanoparticles. The SPR is similar in both samples but slightly more red shifted and broadened, indicating a minimally higher distribution of sizes and decrease in particle size for sample **Ag–N1-500**.

The XPS measurements of films **N1-400**, **N1-500**, **N2-400** and **N2-500** show TiO$_2$ with a small amount of nitrogen *ca.* 1%. Ti 2p readings were observed at 458.1 eV and O 1s peaks at 529.4 eV. The N 1s peak appears at 400.0 eV indicating that the dopant has entered the interstitial site rather than the substitutional site at ~397 eV.[12,14,43] In all cases the quantity of nitrogen is close to the resolution of the machine so is hard to evaluate quantitatively. It has been shown that low concentrations of nitrogen dopant lead to higher photocatalytic activity.[12,14,15,43–47] Interstitial nitrogen is favourable when considering visible light photocatalysis as these

promote oxygen vacancies more than the substitutional doping, though much careful control is needed for the targeted interstitial doping of TiO_2.[12,14,43,46–49] There was no appreciable difference between the different samples in terms of the nitrogen content.

AFM (Fig. 5) was used to show the surface morphology and to see the nanoparticles of silver that were present. It was noted that the silver coverage was ~11% with large surface bound silver nanoparticles. The dimpled morphology of the TiO_2 surface is characteristic of such films prepared by sol–gel methods.

3.2 Functional testing

Water contact angle measurements were taken to measure photoinduced hydrophilicity. The measurements were taken after three different irradiation conditions. Samples were stored in the dark, wrapped in clean aluminium foil for >72 hours prior to the "dark" readings. Samples were then irradiated using a white light or a UV lamp ($\lambda = 365$ nm) for 2 hours before further measurements were taken.

The results show the phenomenon of visible light induced superhydrophilicity (water contact angle < 10°) in the N– and Ag–TiO_2 films. There is also evidence of superhydrophilicity arising without the need for light activation. The presence of superhydrophilicity is usually associated with a light activated cleaning effect[50] but could also be due to the porosity of the surface. Some authors use water contact angle measurements as a proof photocatalytic properties rather than an indicator of likely photocatalytic effects when, as evidenced here, it is clearly only an indicator of the potential photocatalytic properties. These films retain their superhydrophilicity even when stored for >72 h in the dark. In one set of tests the samples were wrapped in aluminium foil and stored in the dark for 1 month and still the water contact angles remained as quoted in Table 2. As expected the light activation does have a lowering effect on the water contact angle, making the samples more superhydrophilic. It is noteworthy that the water contact angles in the dark for the silver

Table 2 Water contact angles for the different samples showing that the higher temperature syntheses produced films that were superhydrophilic without the presence of light activation. Also given are the values for pure TiO_2 and silver loaded TiO_2.[19] Angles of <5° are difficult to measure reliably using a side on projection

Sample	Dark	White	UV
N1-400	14°	<5°	<5°
N1-500	6°	<5°	<5°
N2-400	8°	<5°	<5°
N2-500	11°	<5°	<5°
Ag–N1-500	50°	<5°	<5°
Ag–N2-400	75°	<5°	<5°
TiO₂	64°	64°	8°
Ag–TiO₂	60°	8°	8°

enhanced samples are considerably higher than those observed for the N–TiO_2 samples that were not enhanced with silver. Additionally, it is noteworthy that the N–TiO_2 films are very different in comparison to the TiO_2 thin films reported previously.[19] The presence of nitrogen in the films has a very positive effect on the lowering of the water contact angle, which could be connected with the photocatalytic ability under the ambient lighting conditions, given that the films would have been clean to start with.

Hydrophilicity or more specifically the interaction between the surface and a droplet of water is a very important factor in the ability of a surface to act as a self-cleaning surface.[51] The photocatalysis loosens dirt from the boundary between the glass and the dirt but it is the superhydrophilicity that allows for the dirt to be easily washed away in a uniform manner that does not leave streaks behind. A superhydrophilic surface that retains its ability to sheet water indefinitely, irrespective of light activation, is therefore highly desired. The results displayed in Table 2 can be compared with the results recorded from a similar piece of work where pure titania was enhanced with island of silver nanoparticles.[19] Here we note that the contact angles of the silver
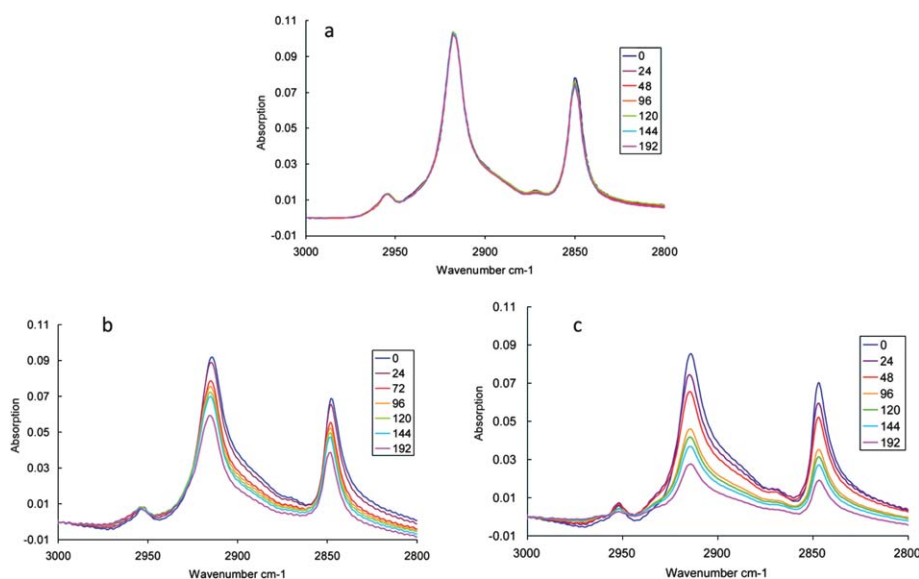

Fig. 6 Photo-oxidation of stearic acid over 192 hours under hospital lighting conditions. (a) Blank microscope slide as a control; (b) **N1-500**, and (c) **N1-500–Ag**. Graphs indicate the concentration of stearic acid on the surface as a factor of time.

Table 3 Rates of stearic acid destruction due to hospital lighting conditions by each film and their silver-coated counterparts. The table shows that the presence of silver nanoparticles increases the photocatalytic activity of each film. The enhancement factor is due to the silver enhancement and calculated by comparing the photodestruction from similar samples

Sample	Molecules destroyed/cm^{-2} h^{-1}	Rate/ molecules cm^{-2} h^{-1}	Sample	Molecules destroyed/cm^{-2} h^{-1}	Rate/ molecules cm^{-2} h^{-1}	Enhancement factor
N1-400	8.10×10^{15}	4.22×10^{13}	**Ag–N1-400**	1.05×10^{16}	5.47×10^{13}	1.29
N1-500	1.63×10^{16}	8.48×10^{13}	**Ag–N1-500**	3.26×10^{16}	1.70×10^{14}	2.00
N2-400	1.95×10^{16}	1.01×10^{14}	**Ag–N2-400**	2.93×10^{16}	1.53×10^{14}	1.51
N2-500	5.85×10^{15}	3.05×10^{13}	**Ag–N2-500**	1.37×10^{16}	7.12×10^{13}	2.34

samples are similar but the pure TiO$_2$ has a significantly higher contact angle on its own in the dark (64°). The N-doping is therefore a significant improvement on the properties of the pure TiO$_2$ reported previously.[19] The silver nanoparticles island formation enhances the light activation but appears to disrupt the inherent dark superhydrophilicity.

Differences in photo-activity were observed between samples of varying nitrogen concentrations, and also between samples heated at varying temperatures. The graphs in Fig. 6 show the absorption IR signal for the C–H stretches in the stearic acid and correspond to ~9.7×10^{15} molecules cm^{-2} of stearic acid for each unit of integrated area.[52] The concentration of stearic acid on the surface is decreased over the 192 hour duration of the experiment indicating that the films are photocatalysts. Sample **N2-400** performs the best, along with sample **N1-500**.

Silver was seen to significantly enhance the rate of stearic acid destruction in all cases. To compare the samples the overall stearic acid destruction and the rates of destruction achieved from each sample have been considered. These are highlighted in Table 3. Of particular interest are the two best performing photocatalysts **N1-500** and **N2-400**. The best catalyst without silver, **N2-400**, showed less enhancement than **N1-500** and was therefore not the best photocatalyst with the silver, **Ag–N1-500**. The worst photocatalyst showed the best enhancement indicating that there may be an optimum ratio of silver to nitrogen. This result is very significant as it shows that an already visible active photocatalyst can have its activity almost doubled when assessed in this way.

Fig. 6 shows the comparison of the raw data for the stearic acid measurements. The blank microscope slide remains unchanged throughout the 192 hours of the irradiation while the N–TiO$_2$ slide and the silver enhanced N–TiO$_2$ samples show significant reduction in the concentration of the stearic acid on the surface resulting from the visible light irradiation. Similar tests were repeated a month later to show that there was little or no depreciation in the films effectiveness, indicating the stability of the samples.

The inactivation of *E. coli* and MRSA deposited on the various coatings is shown in Fig. 7. In both cases the best photocatalysts were used, *i.e.* **Ag–N1-500** and **Ag–N2-400**. Neither coating **N1-500** nor **N2-400** resulted in any detectable antibacterial effect either in the dark or under white light. When silver was added, both coating **Ag–N1-500** and **Ag–N2-400** showed dark and light lethality as the surviving cells on samples stored in the dark were fewer than on the control in both cases. The antimicrobial properties of the samples containing silver were enhanced when exposed to white light as no living *E. coli* cells were detectable and a reduction of about 2 log$_{10}$ for MRSA was achieved, compared to uncoated samples. These results show that samples without silver were not capable of killing *E. coli* or MRSA after 5 hours of exposure to white light, however, when silver was present, the samples had both lethal properties caused by silver (dark toxicity) and light-activated antimicrobial characteristics that are enhanced by the presence of silver. The dark toxicity of both samples was comparable as the amount of silver deposited and is similar in both cases; however *E. coli* was more vulnerable to silver than MRSA. Both samples behaved comparably and could therefore not be differentiated in terms of their antimicrobial toxicity. When compared to samples of pure TiO$_2$ there is an interesting increase in activity. Similar samples with no nitrogen doping showed a 2.5 log kill for EMRSA-16 under similar lighting conditions in 12 hours,[19] compared to a 2 log kill in 5 hours. The kill for *E. coli* was equally remarkable with a 7 log kill in 5 hours compared to a 6 log kill in 12 hours.[19]
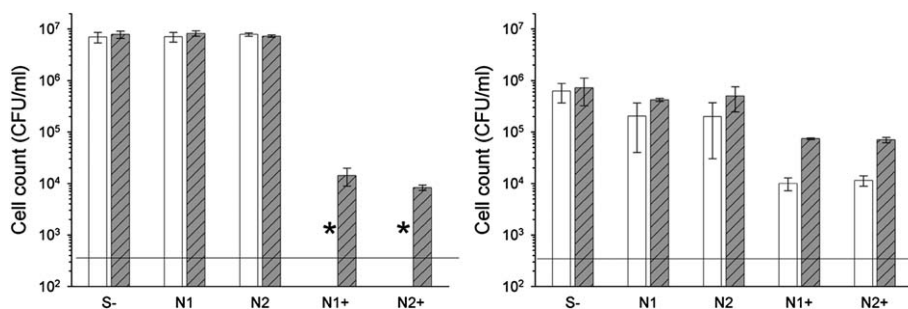

Fig. 7 *E. coli* (a), and MRSA (b) concentration after 5 hours of irradiation with white light (white column) or in the dark (grey patterned column). The horizontal line represents the detection limit; * indicates a concentration below the detection limit; S- is the control glass (uncoated). N1 refers to sample **N1-500**, N2 refers to **N2-400** and the + refers to the presence of silver islands on the surface, *i.e.* **N1-500–Ag** and **N2-400–Ag** respectively.

The silver on its own shown by comparing the dark kills on *E. coli* was about half as effective for the shorter time period.

Generally Gram-negative bacteria are more resistant to decontamination techniques;[53,54] in this work the overall reduction is higher for *E. coli* than MRSA and it caused by the higher sensitivity to silver of such microorganism. Furthermore, it is also noticeable than the surface concentration of *E. coli* did not decrease from the initial value of about 10^7 CFU ml^{-1} after 5 hours, whilst MRSA was reduced to 10^6 CFU ml^{-1} after the same length of time on the control samples. When suspended in a liquid without nutrients, microorganisms gradually die due to starvation; phosphate buffer solution prevents cell lyses but it is not capable of preventing starvation. The reduction in living MRSA cells is caused by this process that is slower in *E. coli* as they are unaffected after the same length of time.

4. Conclusions

The use of silver nano-island formations to enhance the properties of visible light photocatalysts, N-doped TiO$_2$ with the nitrogen in the interstitial site, has been investigated using stearic acid as a model for general dirt and bacteria. Water contact angles show the modified TiO$_2$ films to be superhydrophilic even when stored in the dark for >30 days indicating a rare form of non-light induced superhydrophilicity as well as enhanced visible light induced superhydrophilicity. Visible light superhydrophilicity is observed in the N–TiO$_2$ samples as well as the Ag–N–TiO$_2$ but not in the pure TiO$_2$ samples. The effects of N-doping and Ag-doping work synergistically and are more effective than any one type of doping in isolation. It has further been shown that these photocatalytic thin films can function as antimicrobial surfaces to help prevent the development of bacterial colonies that act as a reservoir for infection, if deployed in healthcare environments. The simplicity of sol–gel synthesis together with the effectiveness of their antimicrobial properties leads to real potential for the application of these surfaces in the control of bacteria such as MRSA.

Acknowledgements

References

1 R. van Grieken, J. Marugán, C. Sordo, P. Martínez and C. Pablos, *Appl. Catal., B*, 2009, **93**, 112–118.
2 P. Wu, R. Xie, K. Imlay and J. K. Shang, *Environ. Sci. Technol.*, 2010, **44**, 6992–6997.
3 G. Hyett, J. A. Darr, A. Mills and I. P. Parkin, *Chem.–Eur. J.*, 2010, **16**, 10546–10552.
4 R. M. Klevens, J. R. Edwards, C. L. J. Richards, T. C. Horan, R. P. Gaynes, D. A. Pollock and D. M. Cardo, *Public Health Rep.*, 2007, **122**(2), 160–166.
5 R. Douglas-Scot, *Centers for Disease Control and Prevention, Division of Healthcare Quality Promotion, National Center for Preparedness D, and Control of Infectious Diseases, Coordinating Center for Infectious Diseases*, 2009.
6 *UK Office of National Statistics*.
7 *Department of Health: Winning Ways: Working together to reduce Healthcare Associated Infection in England*, 2003.
8 A. Mills, N. Elliott, I. P. Parkin, S. O'Neill and R. J. H. Clark, *J. Photochem. Photobiol., A*, 2002, **151**, 171–179.
9 S. A. O'Neill, I. P. Parkin, R. J. H. Clark, A. Mills and N. Elliott, *J. Mater. Chem.*, 2003, **13**, 56–60.
10 R. Asahi, T. Morikawa, T. Ohwaki, K. Aoki and Y. Taga, *Science*, 2001, **293**, 269–271.
11 Y. Suda, H. Kawasaki, T. Ueda and T. Ohshima, *Thin Solid Films*, 2004, **453–454**, 162–166.
12 C. W. H. Dunnill, Z. A. Aiken, J. Pratten, M. Wilson, D. J. Morgan and I. P. Parkin, *J. Photochem. Photobiol., A*, 2009, **207**, 244–253.
13 C. W. Dunnill, Z. A. Aiken, A. Kafizas, J. Pratten, M. Wilson, D. J. Morgan and I. P. Parkin, *J. Mater. Chem.*, 2009, **19**, 8747–8754.
14 C. W. Dunnill and I. P. Parkin, *Chem. Vap. Deposition*, 2009, **15**, 171–174.
15 C. W. Dunnill, Z. A. Aiken, J. Pratten, M. Wilson and I. P. Parkin, *Chem. Vap. Deposition*, 2010, **16**, 50–54.
16 A. Kafizas, C. W. Dunnill and I. P. Parkin, *J. Mater. Chem.*, 2010, **20**, 8336–8349.
17 A. Kafizas, C. W. Dunnill and I. P. Parkin, *Phys. Chem. Chem. Phys.*, 2011, DOI: 10.1039/c1cp20624a.
18 C. Di Valentin, E. Finazzi, G. Pacchioni, A. Selloni, S. Livraghi, M. C. Paganini and E. Giamello, *Chem. Phys.*, 2007, **339**, 44–56.
19 C. W. Dunnill, K. Page, Z. A. Aiken, S. Noimark, G. Hyett, A. Kafizas, J. Pratten, M. Wilson and I. P. Parkin, *J. Photochem. Photobiol., A: Chemistry*, 2011, **113**, 220/2-3.
20 K. Pomoni, A. Vomvas and C. Trapalis, *Thin Solid Films*, 2008, **516**, 1271–1278.
21 Y. Cong, J. Zhang, F. Chen and M. Anpo, *J. Phys. Chem. C*, 2007, **111**, 6976–6982.
22 J. Wang, W. Zhu, Y. Zhang and S. Liu, *J. Phys. Chem. C*, 2006, **111**, 1010–1014.
23 M. Kawashita, S. Tsuneyama, F. Miyaji, T. Kokubo, H. Kozuka and K. Yamamoto, *Biomaterials*, 2000, **21**, 393–398.
24 K. Page, R. G. Palgrave, I. P. Parkin, M. Wilson, S. L. P. Savin and A. V. Chadwick, *J. Mater. Chem.*, 2007, **17**, 95–104.
25 K. Page, M. Wilson and I. P. Parkin, *J. Mater. Chem.*, 2009, **19**, 3819–3831.
26 N. Narband, M. Uppal, C. W. Dunnill, G. Hyett, M. Wilson and I. P. Parkin, *Phys. Chem. Chem. Phys.*, 2009, **11**, 10513–10518.
27 W. Kubo and T. Tatsuma, *J. Mater. Chem.*, 2005, **15**, 3104–3108.
28 K. Selvam, M. Annadhasan, R. Velmurugan and M. Swaminathan, *Bull. Chem. Soc. Jpn.*, 2010, **83**, 831–837.
29 D. Wang, F. Zhou, C. Wang and W. Liu, *Microporous Mesoporous Mater.*, 2008, **116**, 658–664.
30 H. Yu, X. Zheng, Z. Yin, F. Tag, B. Fang and K. Hou, *Chin. J. Chem. Eng.*, 2007, **15**, 802–807.
31 Q. L. Feng, J. Wu, G. Q. Chen, F. Z. Cui, T. N. Kim and J. O. Kim, *J. Biomed. Mater. Res.*, 2000, **52**, 662–668.
32 V. Decraene, J. Pratten and M. Wilson, *Appl. Environ. Microbiol.*, 2006, **72**, 4436–4439.
33 S. Perni, C. Piccirillo, A. Kafizas, M. Uppal, J. Pratten, M. Wilson and I. Parkin, *J. Cluster Sci.*, 2010, **21**, 427–438.
34 S. Perni, C. Piccirillo, J. Pratten, P. Prokopovich, W. Chrzanowski, I. P. Parkin and M. Wilson, *Biomaterials*, 2009, **30**, 89–93.
35 S. Perni, J. Pratten, M. Wilson, C. Piccirillo, I. P. Parkin and P. Prokopovich, *J. Biomater. Appl.*, 2011, **387**, 25/5.
36 S. Perni, P. Prokopovich, C. Piccirillo, J. Pratten, I. P. Parkin and M. Wilson, *J. Mater. Chem.*, 2009, **19**, 2715–2723.
37 C. Piccirillo, S. Perni, J. Gil-Thomas, P. Prokopovich, M. Wilson, J. Pratten and I. P. Parkin, *J. Mater. Chem.*, 2009, **19**, 6167–6171.
38 M. Rai, A. Yadav and A. Gade, *Biotechnol. Adv.*, 2009, **27**, 76–83.
39 S. Noimark, C. W. Dunnill, M. Wilson and I. P. Parkin, *Chem. Soc. Rev.*, 2009, **38**, 3435–3448.
40 R. Swanepoel, *J. Phys. E: Sci. Instrum.*, 1983, **16**, 1214.
41 J. Tauc, *Mater. Res. Bull.*, 1970, **5**, 721–729.
42 J. Tauc, *Mater. Res. Bull.*, 1968, **3**, 37–46.
43 C. W. Dunnill and I. P. Parkin, *Dalton Trans.*, 2011, **40**, 1635–1640.
44 O. Diwald, T. L. Thompson, E. G. Goralski, S. D. Walck and J. T. Yates, *J. Phys. Chem. B*, 2004, **108**, 52–57.
45 A. V. Emeline, V. N. Kuznetsov, V. K. Rybchuk and N. Serpone, *Int. J. Photoenergy*, 2008, **2008**, 258394.
46 H. Irie, Y. Watanabe and K. Hashimoto, *J. Phys. Chem. B*, 2003, **107**, 5483–5486.
47 H. M. Yates, M. G. Nolan, D. W. Sheel and M. E. Pemble, *J. Photochem. Photobiol., A*, 2006, **179**, 213–223.
48 A. Kafizas, S. Kellici, J. A. Darr and I. P. Parkin, *J. Photochem. Photobiol., A*, 2009, **204**, 183–190.

49 T. Okato, T. Sakano and M. Obara, *Phys. Rev. B: Condens. Matter*, 2005, **72**, 115124.

50 T. Zubkov, D. Stahl, T. L. Thompson, D. Panayotov, O. Diwald and J. T. Yates, *J. Phys. Chem. B*, 2005, **109**, 15454–15462.

51 I. P. Parkin and R. G. Palgrave, *J. Mater. Chem.*, 2005, **15**, 1689–1695.

52 A. Mills and J. Wang, *J. Photochem. Photobiol., A*, 2006, **182**, 181–186.

53 S. Perni, D. W. Liu, G. Shama and M. G. Kong, *J. Food Prot.*, 2008, **71**, 302–308.

54 S. Perni, G. Shama and M. G. Kong, *J. Food Prot.*, 2008, **71**, 1619–1625.

This journal is © The Royal Society of Chemistry 2011

J. Mater. Chem., 2011, **21**, 11854–11861 | 11861